Applications of Supercapacitor Energy Storage for a Wave Energy Converter System

Dónal B. Murray[1], M. G. Egan[1], J. G. Hayes[1] and D. L. O'Sullivan[2]

[1]Department of Electrical and Electronic Engineering,
University College Cork,
Ireland.
E-mail: donalm@rennes.ucc.ie

[2]Hydraulics and Maritime Research Centre,
University College Cork,
Ireland.

Abstract

As wave energy converters (WECs) continue their development, improved performance using various energy storage options are constantly being examined.

This paper describes the applications of an energy storage system based on supercapacitors in a full-scale, grid-connected offshore WEC. The following areas are examined: Minimisation of the output power fluctuations; start sequences for the machine; and Low-Voltage Ride-Through (LVRT) capability. Focus is placed on ensuring a component lifetime greater than the maintenance period of the WEC. The investigation is based on a Backward-Bent-Duct Buoy (BBDB) Oscillating Water Column (OWC) using a Wells turbine connected to a Permanent-Magnet Synchronous Machine (PMSM) as the power take-off. The full system is modelled in Simulink using real sea data, and results are shown.

Keywords: Lifetime, LVRT, supercapacitors, WEC

Nomenclature

A	=	Effective area of the capacitor plates
C	=	Capacitance
d	=	Separation distance
ε	=	Permittivity of the dielectric
$\hat{i}_a$	=	Peak phase current
I_c	=	Capacitor current
i_d, i_q	=	Direct and quadrature axis currents
J	=	Turbine inertia
λ	=	Flux linkage
L_g	=	Grid inductance
L_s	=	Stator inductance
ω_e	=	Electrical frequency
ω_m	=	Mechanical speed
p	=	Pole pairs
P	=	Output power
P_{max}	=	Maximum available output power
R_{esr}	=	Equivalent series resistance
R_{epr}	=	Equivalent parallel resistance
R_g	=	Grid resistance
R_s	=	Stator resistance
t	=	Time
T_{em}	=	Electromagnetic torque
$\hat{V}_a$	=	Peak grid phase voltage
v_d, v_q	=	Direct and quadrature axis voltages
$\hat{V}_{inv}$	=	Peak inverter phase voltage
V_{max}	=	Maximum rated voltage
V_{min}	=	Minimum rated voltage
W_{superc}	=	Energy capacity of the supercapacitors
$W_{turbine}$	=	Energy of the rotating turbine
X_g	=	Grid reactance

1 Introduction

1.1 Wave energy

While wave energy offers so much promise in being a leading source of renewable energy, the technology is still in its infancy and the industry is as yet heavily reliant on government funding and incentives. Although many scaled wave test devices have been built, full-scale prototypes are rare and no commercial solution exists.

There are many different types of WECs currently being developed, and most experience the same power take-off (PTO) issues. This paper investigation is based on the oscillating water column (OWC) WEC. The input pneumatic power in an OWC has a fundamentally large variation as the pressure drop across the turbine passes through zero in each wave period and the air flow reverses. The fact that there is no pneumatic power for a time during every wave is the defining difference between OWC WECs and the wind turbine industry from an electrical engineering perspective.

1.2 Previous strategies for WEC power smoothing

The concept of aggregating the output from many WECs in a wave farm to decrease power variation has been examined in [1], although it is recognised that the development of a smoother output from an individual WEC would also improve this process.

The topic of using energy storage systems (ESS) for minimisation of output power fluctuations in individual WECs has been discussed in [2–5]. In these papers, flywheels, turbine inertia, batteries, and Superconducting Magnetic Energy Storage (SMES) systems are utilised.

In an offshore WEC, space and weight are limited as the structure is specially constructed to interact with the waves in order to achieve maximum power extraction for a particular site. Therefore long-term energy storage options such as hydrogen production, Compressed-Air Energy Storage (CAES), Battery Energy Storage Systems (BESS), and pumped hydroelectric are bulky and unsuitable for the current application.

The short-term options consist of SMES, supercapacitors, flywheels, and batteries. Flywheels and supercapacitors are the most reliable and robust of these technologies and while using flywheels and system inertia have been investigated for WECs, supercapacitors have to date not been examined in detail.

1.3 Objectives

This paper explores the use of supercapacitor energy storage in a full-scale grid-connected offshore OWC WEC. The overall topology is shown in Fig. 1, where a Wells turbine utilising NACA0015 blades is coupled to a Permanent-Magnet Synchronous Machine (PMSM) as the power take-off.

Supercapacitor systems are reviewed and potential applications are discussed. Descriptions and results of Simulink modelling using real sea data are then presented.

2 Supercapacitors in WECs

2.1 Overview of supercapacitors

Supercapacitors are also known variously as electric double layer capacitors, ultracapacitors, and Electrochemical Double Layer Capacitors (EDLC). They have a very high energy density and are governed by the same equations as all capacitors. The value of capacitance is given by (1).

$$C = \frac{\varepsilon A}{d} \tag{1}$$

Supercapacitors use a porous carbon-based electrode and the surface area of this porous material is around 2,000,000 m^2/kg. The charge separation distance (less than 10 angstroms) is much smaller than what can be accomplished using conventional dielectric materials. These properties give the supercapacitors their extremely high capacitance in accordance with (1), with values reaching 5000 F. Unfortunately the electrodes have a small breakdown voltage and voltage ratings in typical supercapacitors do not go above 2.7 V. In order to achieve higher voltages, individual cells are connected in series.

While supercapacitors cannot compete with batteries in terms of energy density, their much longer cycle life, power density, operational temperature range, and ability to fully discharge make them an energy storage option that must be considered in many applications. Coupled with this, supercapacitors have charge/discharge efficiencies ranging from 0.85 to 0.98 [6].

Equivalent circuit models for supercapacitors have been examined in [7–9]. They include the classical RC model, parallel-branch model, transmission-line model, and the multi-branch model. This paper uses the classical RC model shown in Fig. 2 which includes the most important parameters, while still allowing processing power to simulate the rest of the system. The equivalent series resistance, R_{esr}, limits the charge/discharge current of the device and contributes to internal heating.The parallel resistance, R_{epr}, simulates the energy loss due to self-discharge.

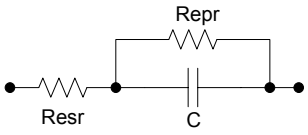

Figure 2: Supercapacitor equivalent circuit used

Research on supercapacitors as an energy storage device for use with renewable energy systems has been explored in [10]. In these references a supercapacitor module was connected, using a bi-directional dc-dc converter, to the dc-link in a Doubly-Fed Induction Generator (DFIG) based wind turbine. The module was sized based on Low-Voltage Ride-Through (LVRT) requirements, and a fuzzy logic control scheme was implemented to smooth power fluctuations and reinforce the dc-bus during transients. Applications with photovoltaics were shown in [11, 12], where the supercapaci-

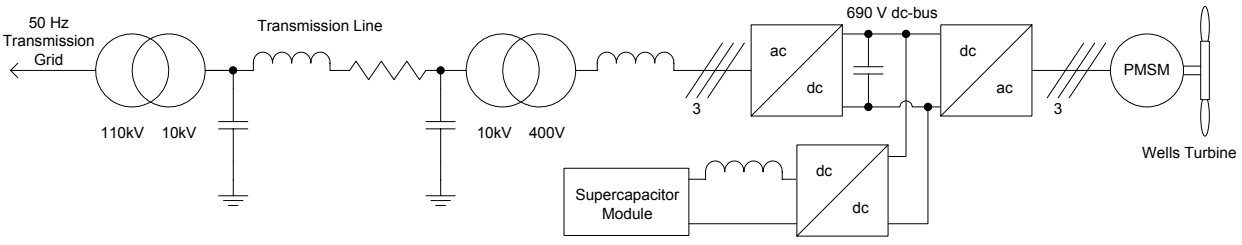

Figure 1: WEC grid-connected system

tors complemented battery storage and improved system performance and battery lifetime.

The ability of supercapacitors to operate at sea for long periods of time was shown in [12]. Supercapacitors have also been used in wind turbine pitch systems, hybrid vehicles, and lift trucks, also demonstrating their robustness.

2.2 Supercapacitor lifetime

Capacitor lifetime is a topic that is often overlooked in papers on supercapacitor energy storage for renewable energies. Supercapacitors do not have a hard failure point to indicate end of life, but rather a maximum deviation from initial parameters. This exact deviation differs among manufacturers but a common reference is a capacitive reduction of 20% or an increase in the R_{esr} of 100% from the initial specified values.

All of the leading manufacturers of supercapacitors quote lifetimes of up to one million cycles or less and it is stated in [13] that cycle depth does not affect this lifetime.

Most papers researching supercapacitor lifetimes focus on voltage and temperature effects, as these are believed to be the determining factors. Due to the large powers involved in power levelling in the offshore WEC, a large amount of heat would be dissipated in the R_{esr} of the supercapacitor module, leading to internal heat generation and further life reduction. According to [14], a temperature increase of 10 °C reduces life expectancy by approximately half. Also, lifetime is halved for each 100 mV above nominal voltage [15]. In these tests the supercapacitor operating voltage was maintained at a constant value for a given temperature, and C and R_{esr} are measured over time.

2.3 Supercapacitors for power smoothing

The average pneumatic input power calculated from typical sea-state data for the fixed speed OWC WEC under consideration in this paper, is 123 kW, while the peak input power is 2.1 MW. Assuming a 50% conversion efficiency from pneumatic to electrical power [16], this results in an average electrical power output of 61.5 kW and gives a rough indication of the expected power requirements for the storage device needed to smooth output power. A typical large supercapacitor power module has a continuous rated power output in the range of 9 kW to 18 kW. Therefore by connecting a number of these modules together, the power requirements can be met.

Maintenance intervals in offshore WECs should be long and not limited by a prototype supercapacitor system. The difficulty in carrying out on-board maintenance on an offshore WEC is highlighted in [17], where docking issues and working in an unstable environment are key concerns. A typical desired interval is five years which gives the desired lifetime of any employed supercapacitor module. An indication of the operational time for an offshore WEC is given in [18], where it is stated that their device is idle for about one third of the year.

A wave period of 10 seconds is typical for most full scale WECs and the examined sea-state in this paper has an average period of 7.6 seconds. Due to the unidirectional turbine torque from the bidirectional airflow in OWCs, the average input pneumatic power period is half this value. From this the required cycle life for a device used for power smoothing over every wave period can be calculated as shown in (2).

$$\begin{aligned} \text{Power period} &= 5\text{ s} \\ \text{Expected cycles} &= 12\text{ cycles/minute} \\ &= 720\text{ cycles/hour} \\ &= 720 \times 5 \times 2/3 \times 365.25 \times 24 \\ &\approx 21{,}000{,}000\text{ cycles/5 years} \end{aligned} \quad (2)$$

Comparing the given one million lifecycle value for supercapacitors with this lifecycle specification, it appears that supercapacitors cannot help attenuate normal operating output power fluctuations. While it can be inferred that reducing the operating voltage will extend cycle lifetime, as yet no data on this topic is available, and it is unknown if 21 million power cycles is attainable.

Some supercapacitor modules require voltage balancing due to capacitive tolerances between cells to ensure no over-voltages take place. The reliability of each of these balancing circuits as well as each low voltage supercapacitor cell placed in series in a module, are key concerns when investigating continued power cycling operation over five years.

More research is needed on these issues before this application of power smoothing can be examined for supercapacitors. However supercapacitors can still make a significant contribution to the development of offshore WECs.

2.4 Supercapacitors for turbine start-up

Wells turbines are not self starting. During start-up in high energy sea-states, considerable energy is required to accelerate the high inertia turbine from rest.

In offshore WEC prototypes currently in operation, this start-up has so far been implemented using on-board batteries. Batteries are high energy density, low power devices that do not benefit from the same cycle life as supercapacitors. Also, high power drain can significantly reduce their lifetime. To ensure the battery is not damaged, it is proposed to use the supercapacitor module as the start-up mechanism. This will ensure the WEC will start rapidly without a grid-side surge and begin generating power once an energetic sea-state is sensed (typically done using a predefined value for rms pressure inside the chamber).

While the power converter used is bi-directional and could theoretically be employed to start the machine, it is preferable to allow power flow in one direction only to help with ratings and minimise cost of safety and protective equipment. This also has advantages from a grid operator perspective, by limiting starting current surge from the grid as well as in terms of the import capacity of the grid connection.

Turbine damping increases as speed increases and this allows the turbine to interact more efficiently with the oscillating air stream. Turbine stall is also reduced. As the turbine gathers speed, more and more input torque will be experienced and aid in the acceleration to the set speed where normal operation can occur.

As seen in Fig. 1 the system topology consists of the generator connected to the grid via full-rated back-to-back PWM voltage-source converters.

The control strategy used for the motoring sequence consists of first setting i_d to zero in the grid-side converter to prevent active power flow through the device. Also, as flux weakening mode will not be used in the PMSM, i_d is set to zero in the machine-side converter.

The machine-side converter controls the speed of the turbine using cascaded speed/current loops. The limit for the inner current loop is initially set to ensure that the current rating of the converter is not exceeded.

The dc-link voltage is maintained at the desired set point by controlling the supercapacitor current. As the machine accelerates due to i_q, the input power increases and the current pulled from the supercapacitor module increases. Once the current rating of the supercapacitor module is reached, it is maintained at this value and control of the dc-link voltage is now achieved using the machine current i_q. This controlled current sets the limit of the inner current loop.

Obtained plots for this scheme are shown in the results section. Total energy flows in the circuit are also observed.

2.5 Supercapacitors for LVRT

The increased proportion of wind turbines in the electrical grid has led to stricter grid codes for these devices. While wave energy is still in the development stage, it is expected to eventually experience the same sort of growth that the wind industry has had over the past 10 years. If these expectations are realised, it will be probable that similar grid codes will be put in place for the wave industry.

A typical grid code can be seen in [19]. It states that wind farm power stations should remain connected to the transmission system for voltage dips on any or all three phases, where the transmission system phase voltage remains above the black line in Fig. 3. In addition to this, these power stations shall provide active power in proportion to the retained voltage and maximise reactive current to the transmission system without exceeding turbine limits.

In a low-voltage event, the ability to transfer power to the grid is limited as it is a function of the grid voltage. If this occurs when the turbine is experiencing high input power, there will be a transient power imbalance and the dc-link voltage will rise dangerously unless controlled. There are four options to ride through the fault: allow the turbine to speed up and curtail power going onto the dc-link, extract the excess power flow onto the dc-bus to an energy storage device, burn off excess energy using a chopper and load bank circuit, or a combination

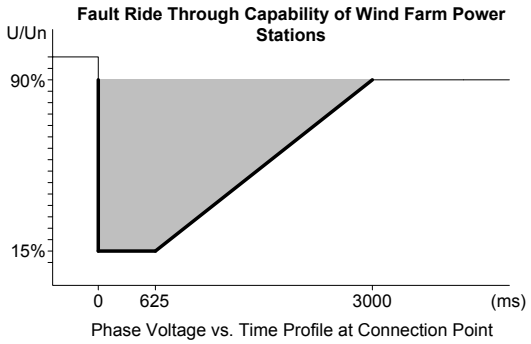

Figure 3: Eirgrid LVRT requirement [19]

of these. The option examined in this paper is a combination of using supercapacitors connected to the dc-link and allowing the turbine to accelerate.

Due to the use of a full rated back-to-back converter, a disturbance in the grid frequency is not an issue. Also, this topology allows control of active and reactive power with the use of the currents i_d and i_q.

The grid code states that the power station should provide active power in proportion to the grid voltage, but for a turbine operated at constant speed, the output power profile corresponds to the fluctuating input pneumatic power. In order to supply a fixed power in proportion to the retained voltage, the current i_d is fixed during the low-voltage event according to (3). Due to difficulties in predicting input energy over a three second period in highly variable sea-states, this value is calculated using worst case conditions to ensure the turbine speed rating is not exceeded during the fault. It is important to ensure that the turbine will not decelerate below the minimum operational speed limit during low energy or high stall events, and that a significant amount of reactive power can be generated (4).

$$P = \frac{3}{2} v_d \, i_d \tag{3}$$

The grid-side current i_q is evaluated to maximise reactive power ensuring that limits for current or inverter voltage are not exceeded according to (4) and (5).

$$\hat{i}_a = \sqrt{{i_d}^2 + {i_q}^2} \tag{4}$$

$$\hat{V}_{inv} = \hat{V}_a + (i_d + j\, i_q)(R_g + j X_g) \tag{5}$$

This method allows for a clear prediction of output power and reactive power from the WEC for all low-voltage events.

The desired dc-link voltage is achieved by controlling the machine i_q, while the supercapacitor module is used to control turbine speed ensuring limits are not exceeded.

In this simulation, a three phase fault is analysed resulting in the most severe voltage profile which the system has to endure. The case where supercapacitors are not used (with no control over turbine speed) is shown, followed by the same conditions using the supercapacitor module. Sea-state data is used to give a typical turbine torque input during the event.

3 OWC system model

3.1 Overview

One of the advantages of the system utilising a Wells turbine in an OWC, is that the high speed bi-directional airflow facilitates the use of shaft speeds that are consistent with most generators and therefore eliminates the need for a gearbox [17, 20].

Wells turbines need to be robust to withstand the lift, drag and axial forces. They are generally high inertia devices, with typical inertia levels up to 500 kg m^2 in full-scale converters [5], with pneumatic to mechanical peak power conversion efficiencies of 60-70%. The simulated Wells turbine uses NACA0015 blades. The diameter of this nine bladed, aluminium turbine is two metres, and it has a hub to tip ratio of 2/3. This gives an inertia of 85 kg m^2 for the device, and a weight of 220 kg. The shaft of the coupled PMSM has an inertia of 10 kg m^2 and the speed for the device was set at 1000 rpm.

In order to draw conclusions from this work, a full-scale grid-connected system was simulated.

As mentioned above, the average input pneumatic power is 123 kW and the peak input power is 2.1 MW. While the optimum rating of generators for use in WECs is an issue that has not yet been addressed fully, the accurate prediction of stall speed in a Wells turbine provides a maximum mechanical power value. In the turbine model used (described below), it is found that there is a maximum input torque value for a given turbine speed before stall occurs and any further increase in input pneumatic power will lead to a torque reduction. The maximum allowed speed for the system was chosen as 1200 rpm, as mechanical stresses on the Wells turbine are a concern above this value. A model of this turbine predicts a maximum input torque of 2305 Nm, and a maximum mechanical output power of 290 kW (this assumes a control scheme that prevents the turbine speed exceeding the specified value). This estimated peak power rating, together with the time-varying sea-state data, enables an appropriately rated permanent-magnet machine to be selected, ensuring that the power fluctuations will not damage the permanent magnets in worst case conditions. Converter current ratings are also selected based on this maximum torque figure.

A permanent-magnet machine is used due to its high efficiency and controllability. It is noted in [17], that a brushless machine is needed in offshore WECs due to impractical maintenance requirements associated with brush replacement. A two level back-to-back power converter decouples the machine from the 50 Hz grid. This brushless machine and converter layout is becoming the topology of choice in the offshore wind industry and therefore this design satisfies the reliability requirements of a WEC.

The full system topology is shown in Fig. 1. The back-to-back converter feeds a local transformer which steps the voltage up to 10 kV. Power is transported to shore via an ac transmission cable, where a larger transformer on land steps the voltage up to 110 kV and feeds power into the transmission grid, assumed to be an infinite bus. This larger transformer rating is to allow the aggregation of the power from 10 such devices, which would make up a small wave farm. While the work did not model the transformers and transmission line in the grid-connection, the full layout is shown for completeness.

3.2 Turbine model

The developed systems are modelled in Simulink using real sea-state data and a Wells turbine model developed in [17]. Pneumatic power is the input to the model and using speed, non-dimensional pressure, and flow, the resultant turbine torque is produced. Typical input pneumatic power from a common sea-state for the site, and the resultant turbine torque when operated at 1000 rpm, are shown in Fig. 4.

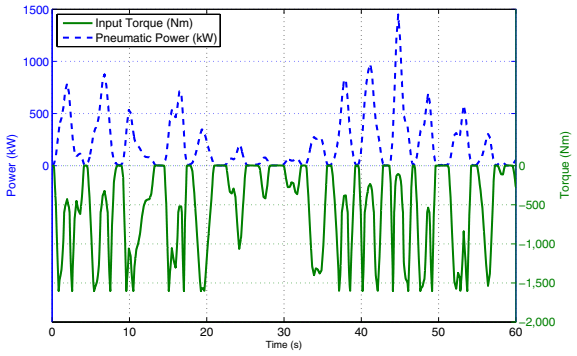

Figure 4: Pneumatic power and resultant turbine torque from typical sea-state data for the full-scale device

3.3 Back-to-back converter model

A Field-Oriented Control (FOC) scheme was developed utilising speed and current PI loops. This operated back-to-back converters using sine wave Pulse-Width Modulation (PWM). The machine-side converter is used to maintain the speed of the turbine at the preset desired value of 1000 rpm. Machine voltages and currents are transformed to d and q-axis variables using the Park transformation. The equation for the electromagnetic torque in a PM machine is shown in (6).

$$T_{em} = \frac{3\,p}{2}\,\lambda_{fd}\,i_q \tag{6}$$

where λ_{fd} is the flux linkage of the stator direct-axis windings due to the flux from the rotor magnets, the d-axis is always aligned with the rotor magnetic axis, and i_q is the quadrature-axis current in the stator windings. This equation is valid for a non-salient machine (assumed in this analysis). As the set point speed is fixed, flux-weakening mode was not used, and i_d was set to zero.

A PI controller uses a speed error to create a reference q-axis current which is directly proportional to machine torque as shown. This machine-side converter control

technique is described in full in [21]. The desired stator d and q-axis voltages are set according to (7) and (8) by using PWM in an ideal inverter.

$$v_d = R_s i_d + L_s \frac{d}{dt} i_d + (-\omega_e L_s i_q) \tag{7}$$

$$v_q = R_s i_q + L_s \frac{d}{dt} i_q + \omega_e \left(L_s i_d + \lambda_{fd}\right) \tag{8}$$

A full switched model of the machine converter was developed in Simulink using the SimPowerSystems library, and the resulting schematic is shown in Fig. 5.

The controller gains for the speed and current loops are calculated using [21].

The grid-side converter is controlled in a similar way, where the dc-link voltage is maintained at a desired level using PI controllers. Any current fed onto the dc-link from the machine is outputted to the grid to maintain a constant dc-link capacitor voltage. The current i_d gives real power out, while i_q can be controlled to meet reactive power requirements. The main control equations, (9) and (10), are shown. The full method is described in detail in [22].

$$v_{d\_des} = -v'_d + (\omega_e L_g i_q + v_d) \tag{9}$$

$$v_{q\_des} = -v'_q - (-\omega_e L_g i_d) \tag{10}$$

where v'_d and v'_q are the outputs of the PI current loop controllers.

The SimPowerSystems Simulink schematic of the grid converter is shown in Fig. 6.

To simulate the systems for periods of time that give an accurate view of the sea-state data, a separate PWM time averaged model without PWM switching was also created using controllable voltage and current sources.

3.4 Supercapacitor converter and control

In order to decouple the supercapacitors from the system and allow full control over their operation, a bi-directional dc-dc converter was used. The supercapacitor module was placed on the low voltage side of the

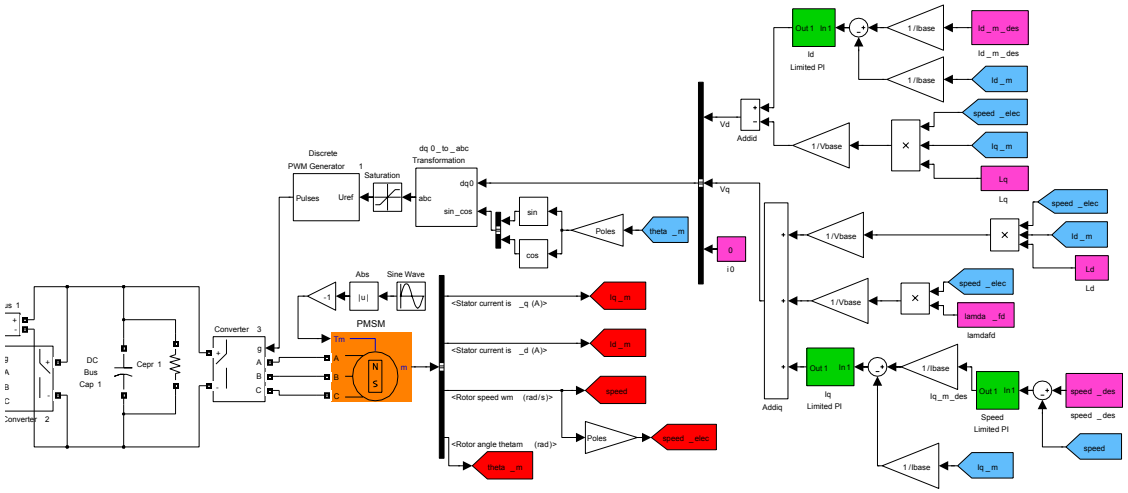

Figure 5: Simulink schematic of the machine-side converter

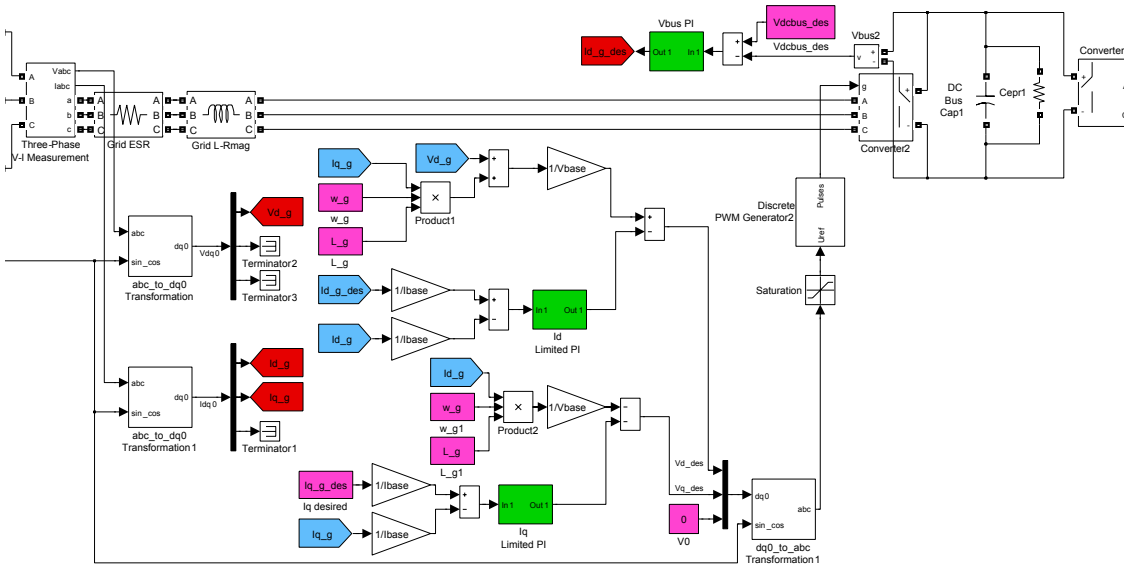

Figure 6: Simulink schematic of the grid-side converter

converter in order to obtain full use of the supercapacitor's voltage and energy range [23]. Also, modules tend to be available with low voltage ratings. The proposed system can be seen in Fig. 1.

One of the objectives of this paper was to power up the system from rest. In order to estimate the capacity of supercapacitors needed, the following equations were used.

$$W_{turbine} = \frac{1}{2} J \omega_m{}^2 \tag{11}$$

$$W_{superc} = \frac{1}{2} C \left(V_{max}{}^2 - V_{min}{}^2 \right) \tag{12}$$

The set point speed for the system is 1000 rpm and the total inertia of coupled masses is 95 kg m^2. From this, the total kinetic energy stored in the system from rest (neglecting friction) is 520 kJ.

The BMOD0063 P125 supercapacitor module, from Maxwell Technologies, was chosen for this project. The standard voltage rating is 125 V, and the capacitance is 63 F. It is common practice to choose the minimum voltage at half the maximum value and then to add a 20% safety margin to the required energy value (to ensure that energy requirements are still satisfied near supercapacitors' end of life). Using (12), the energy available from the module when fully charged is around 370 kJ. Therefore two such modules in series give 591 kJ at 80% capacitance. This would provide the required energy level and have enough excess energy to overcome heating losses in parasitic elements and friction losses in the turbine. Given the capacitance tolerance of the modules, voltage balancing is required.

This voltage range of 125 V - 250 V is high enough for the bi-directional dc-dc converter to operate when connected to the 690 V dc-bus. The specifications of a single BMOD0063 P125 module, are shown in Table 1.

Table 1: Parameters of the supercapacitor module [24]

Maxwell Technologies BMOD0063 P125	
Surge voltage (V)	135
Operating temperature range	$-40\,^{\circ}$C to $+65\,^{\circ}$C
Capacitance tolerance	$+20\%$ / -0%
Cycle life (cycles)	1,000,000
R_{esr}, DC (mΩ)	18
Mass (kg)	59.5
Max continuous current (A)	150
Max peak current, 1 second (A)	750

It is specified in [24] that, after 30 days, 50% of the initial voltage remains. The parallel resistance shown in the equivalent circuit above would then be calculated to be about 120 kΩ, using (12) and (13). This module employs Maxwell's Voltage Management System (VMS), assumed ideal for this paper.

$$R_{epr} = \frac{-(t_2 - t_1)}{ln\left(\frac{V_2}{V_1}\right) C} \tag{13}$$

Selection of the filter inductance in the above circuit is important as it operates in both buck and boost mode. Minimisation of this device using variable switching frequency is examined in [25], while an extra filter stage comprising of a low value inductance is shown in [26].

The supercapacitor's capacitance is quoted at dc and this rapidly reduces to a very low value beyond 100 Hz [26]. Therefore, the supercapacitors cannot significantly attenuate the voltage ripple generated by switch mode converters and filtering is required. It is recommended in [26] to use a low value inductance in series with the supercapacitors, to attenuate this ripple and to increase lifetime.

Maximum output power available from supercapacitors is given by (14).

$$P_{max} = \frac{1}{4} \frac{V^2}{R_{esr}} \tag{14}$$

While this is calculated to be 434 kW at the minimum operating voltage, for the lifetime reasons outlined above, it is much lower than this in practice to ensure the temperature of the module remains within specified limits. From the data above, the maximum output power ranges from 73.5 kW to 167 kW for a maximum of one second, or 18 kW to 36.5 kW corresponding to the rated maximum continuous current.

The operating voltage of the supercapacitor module during WEC operation was chosen at half the usable energy range which is 197.6 V. Using (15), the maximum voltage of the supercapacitor modules when charged at rated current for three seconds and with 80% capacitance was checked to ensure ratings would not be exceeded during LVRT. This was found to be 239 V.

$$I_c = C \frac{dV}{dt} \tag{15}$$

The stall value of the system was used to evaluate the maximum power input. Then power and energy values throughout the whole of the low-voltage event were calculated and balanced to evaluate the current i_d, ensuring rated speed of 1200 rpm would not be exceeded. This was calculated to be 265 A, which gave a grid energy output of 174 kJ. Due to the one second supercapacitor current rating, power requirements during the most severe part of the fault could be satisfied by the supercapacitor module and grid power, and the turbine would not accelerate. Turbine inertia helped balance worst case power requirements after this and it was noted that maximum power input increased due to the increased speed and increased stall torque. Ratings were then checked for the case where no input wave energy occurs during the fault to ensure that turbine speed remains above the minimal operating speed of 850 rpm.

4 Results

Results from the start-up control strategy using supercapacitors are illustrated in Fig. 7 and Fig. 8.

It can be seen from this that it takes 10.5 seconds to accelerate the turbine to the set speed from rest. As expected, the turbine input torque increases as the speed increases beyond the stall value. The ratings for i_q and

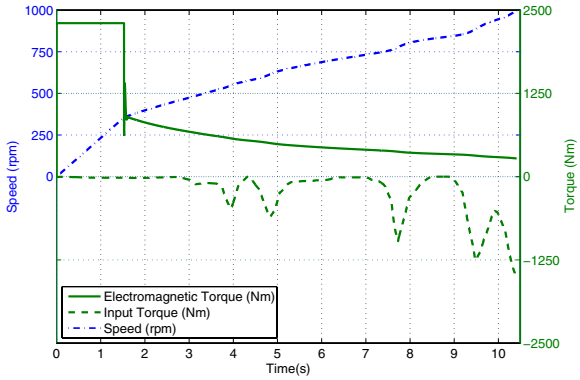

Figure 7: Speed, input torque and electromagnetic torque versus time during turbine start-up with typical sea-state data

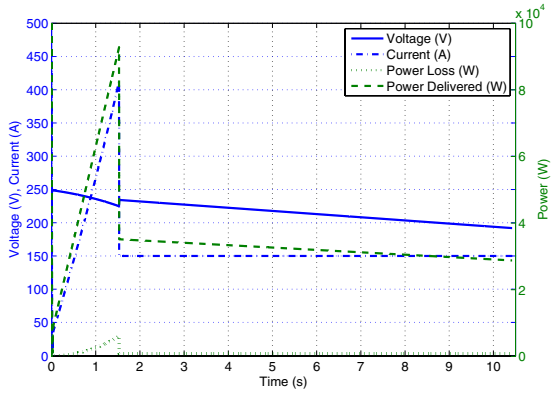

Figure 8: Supercapacitor voltage, current, power, and power loss during turbine start-up

capacitor current are also observed in the graph. It is specified in Table 1 that the continuous rated current can be exceeded for one second up to a value of 750 A. This was taken into account before control of the dc-link voltage was taken over by the machine i_q from the supercapacitor module. Two tests were carried out. In the first test, the input torque was set to zero, and in the second test, real sea data was used to produce an accurate input torque during start-up. The first test demonstrates worst case conditions as low input wave energy events occur in all sea-states and one could occur after the start signal. The energy values are shown in Table 2.

It is noted that the energy of the rotating turbine is approximately equal to the energy supplied by the supercapacitors plus turbine, minus losses. The small difference is due to the energy contained in the inductances of the machine.

Plots from the LVRT analysis are shown. The transient is simulated for four seconds, and voltage collapse begins at 0.75 seconds. The voltage profile is seen in Fig. 9, and the output grid current, power and reactive power are seen in Fig. 10 and Fig. 11 respectively. Maximum reactive power is outputted while satisfying current and voltage ratings.

Fig. 12 illustrates the corresponding turbine speed

Table 2: Energy supplied and lost in the system during motoring (assuming an ideal converter)

	Motoring without P_{pneu}	**Motoring with P_{pneu}**
Time taken (s)	17.19	10.42
	Energy at full speed (J)	
	520896	
	Energy supplied (J)	
Supercapacitor	554836	371182
P_{pneu}	0	175380
	Energy lost (J)	
Supercapacitor R_{esr}	15847	10369
Generator R_s	14631	13669
Generator friction	3369	1567
Dc-bus capacitor R_{epr}	82	50
Supercapacitor R_{epr}	6	4

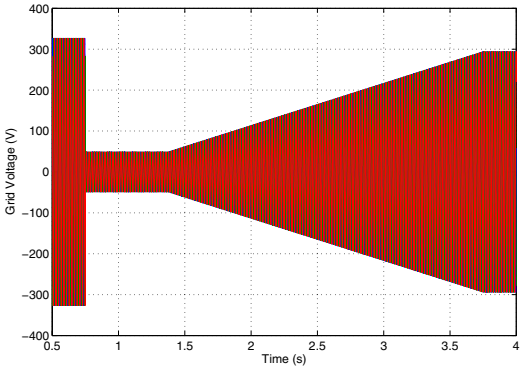

Figure 9: Grid voltage during LVRT event

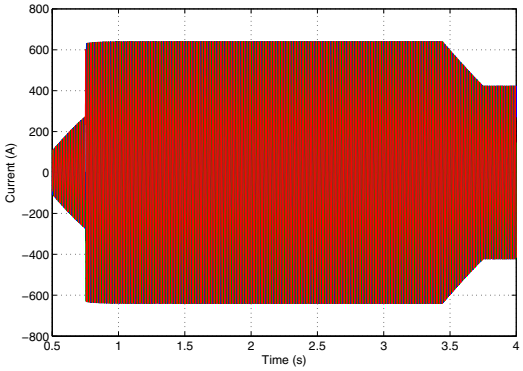

Figure 10: Grid current during LVRT event

and input torque for the case without supercapacitor energy storage. It is seen that a significant overspeed occurs.

Fig. 13 and Fig. 14, demonstrate the situation in which the supercapacitor module is employed. The supercapacitor current and voltage ratings are satisfied, and turbine speed remains within limits. The same input

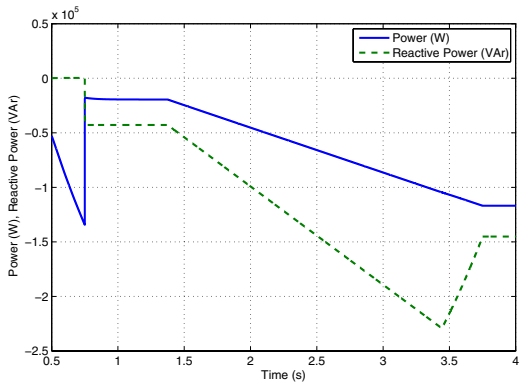

Figure 11: Grid power and reactive power during LVRT event

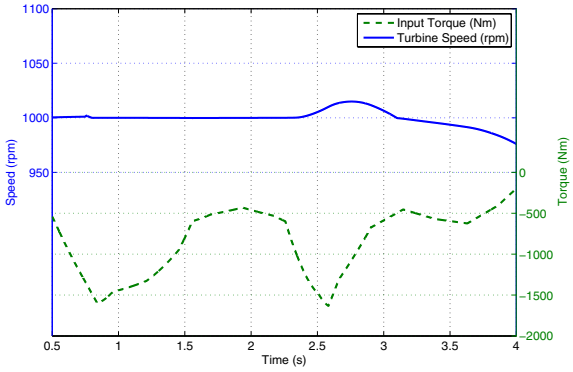

Figure 13: Turbine speed and input torque during LVRT event with supercapacitors

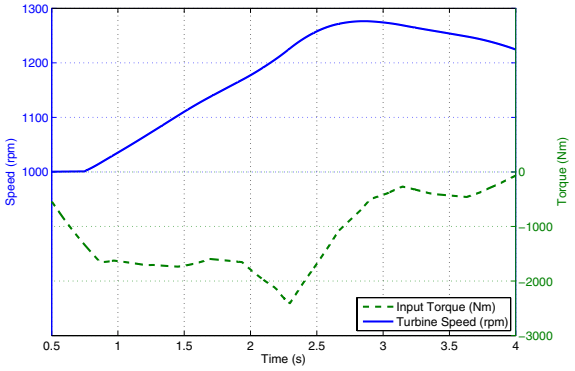

Figure 12: Turbine speed and input torque during LVRT event without supercapacitors

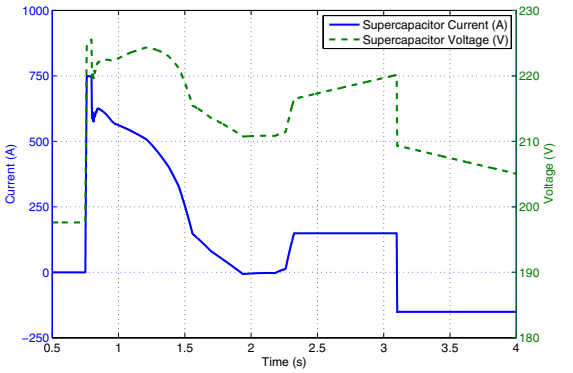

Figure 14: Supercapacitor voltage and current during LVRT event

wave data is applied to both tests, and stall is seen to occur in Fig. 13 as turbine speed is reduced.

5 Conclusions

This paper reviewed the use of supercapacitor energy storage in renewable energy systems. It was shown that a significant increase in supercapacitor cycle lifetime needs to be demonstrated before the application of power smoothing can be researched fully. From present specifications, supercapacitor lifetimes would be too short to satisfy maintenance and reliability requirements.

Two applications of supercapacitors were shown using a full sized WEC model. By employing supercapacitors to power-up the turbine, starting surge for a wave farm can be minimised. Also, by contributing towards LVRT, future grid codes may be satisfied and redundancy is built into the system.

Other uses of the supercapacitors which can be explored are regenerative braking of the turbine during normal or emergency shutdown.

Acknowledgements

This work has been sponsored by IRCSET through the Embark Initiative. The author would also like to thank those in the Hydraulics and Maritime Research Centre at UCC.

References

[1] M. Molinas, O. Skjervheim, P. Andreasen, T. Undeland, J. Hals, T. Moan, and B. Sorby. Power electronics as grid interface for actively controlled wave energy converters. *International Conference on Clean Electrical Power, 2007. ICCEP '07*, pages 188–195, May 2007.

[2] S. Muthukumar, S. Kakumanu, S. Sriram, R. Desai, A. A. S. Babar, and V. Jayashankar. On minimizing the fluctuations in the power generated from a wave energy plant. *2005 IEEE International Conference on Electric Machines and Drives*, pages 178–185, 15 May 2005.

[3] S. Muthukumar, S. Kakumanu, S. Sriram, and V. Jayashankar. Energy storage considerations for a stand-alone wave energy plant. *2005 IEEE International Conference on Electric Machine and Drives*, pages 193–198, 15 May 2005.

[4] D. Kiran, A. Palani, S. Muthukumar, and V. Jayashankar. Steady grid power from wave energy. *IEEE Transaction on Energy Conversion*, 22, Issue 2:539–540, June 2007.

[5] A. F. de O. Falcao. Control of an oscillating-water-column wave power plant for maximum energy produc-

tion. *Applied Ocean Research*, Vol. 24, Issue 2:73–82, April 2002.

[6] H. Douglas and P. Pillay. Sizing ultracapacitors for hybrid electric vehicles. *31st Annual Conference of IEEE Industrial Electronics Society, 2005. IECON 2005*, 6-10 November 2005.

[7] L. Shi and M. L. Crow. Comparison of ultracapacitr electric circuit models. *2008 IEEE Power and Energy Society General Meeting - Conversion and Delivery of Electrical Energy in the 21st Century*, pages 1–6, 20-24 July 2008.

[8] T. Wei, X. Qi, and Z. Qi. An improved ultracapacitor equivalent circuit model for the design of energy storage power systems. *International Conference on Electrical Machines and Systems, 2007. ICEMS*, pages 69–73, 8-11 October 2007.

[9] Y. Y. Yao, D. L. Zhang, and D. G. Xu. A study of supercapacitor parameters and characteristics. *International Conference on Power System Technology, 2006. PowerCon 2006*, pages 1–4, October 2006.

[10] C. Abbey and G. Joos. Supercapacitor energy storage for wind energy applications. *IEEE Transactions on Industry Applications*, Vol. 43, Issue 3, June 2007.

[11] M. E. Glavin, P. K. W. Chan, S. Armstrong, and W. G. Hurley. A stand-alone photovoltaic supercapacitor battery hybrid energy storage system. *13th Power Electronics and Motion Control Conference, 2008. EPE-PEMC 2008*, pages 1688–1695, 1-3 September 2008.

[12] D. V. Weeren, H. Joosten, R. Scrivens, and A. Schneuwly. Ultracapacitors double operational life of wave measurement buoys. available online at www.maxwell.com/ultracapacitors, Accessed 10th April 2009.

[13] Maxwell Technolgies. Top 10 reasons for using ultracapacitors in your system designs, white paper. www.maxwell.com, Accessed 10th April 2009.

[14] D. Linzen, S. Buller, E. Karden, and R. W. De Doncker. Analysis and evaluation of charge-balancing circuits on performance, reliability, and lifetime of supercapacitor systems. *IEEE Transactions on Industry Applications*, Vol. 41, Issue 5:1135–1141, October 2005.

[15] EPCOS. Ultracap data sheet collection 2005. available online at www.epcos.com.

[16] R. Curran, T. J. T. Whittaker, and T. P. Stewart. Aerodynamic conversion of ocean power from wave to wire. *Energy Conversion and Management*, Vol. 39, Number 16:1919–1929, November 1998.

[17] D. L. O'Sullivan and A. W. Lewis. Generator selection for offshore oscillating water column wave energy converters. *13th Power Electronics and Motion Control Conference, 2008. EPE-PEMC 2008.*, pages 1790–1797, 1-3 September 2008.

[18] G. P. Harrison and A. R. Wallace. Sensitivity of wave energy to climate change. *IEEE Transaction on Energy Conversion*, Vol. 20, Issue 4:870–877, December 2005.

[19] Eirgrid. Eirgrid grid code, version 3.2. available online at www.eirgrid.com, December 2008.

[20] M. A. Mueller, H. Polinder, and N. Baker. Current and novel electrical generator technology for wave energy converters. *IEEE International Electric Machines & Drives Conference 2007. IEMDC '07*, Vol. 2:1401–1406, May 2007.

[21] N. Mohan. *Advanced Electric Drives: Analysis, Control and Modeling using Simulink*. MNPERE, 2001.

[22] R. Pena, J. C. Clare, and G. M. Asher. Doubly fed induction generator using back-to-back pwm converters and its application to variable-speed wind-energy generation. *Electric Power Applications, IEE Proceedings-*, Vol. 143, Issue 3:231–241, May 1996.

[23] W. Li, G. Joos, and C. Abbey. A parallel bidirectional dc/dc converter topology for energy storage systems in wind applications. *Conference Record of the 2007 IEEE Industry Applications Conference, 2007*, pages 179–185, 23-27 September 2007.

[24] Maxwell Technologies. Bmod0063 ultracapacitor datasheet. www.maxwell.com, Accessed April 2009.

[25] T. Wei, S. Wang, and Z. Qi. A supercapacitor based ridethrough system for industrial drive applications. *International Conference on Mechatronics and Automation, 2007. ICMA 2007*, pages 3833–3837, 5-8 August 2007.

[26] S. Basu and T. M. Undeland. A novel design scheme for improving ultra-capacitor lifetime while charging with switch mode converters. *IEEE Power Electronics Specialists Conference, 2008. PESC 2008*, pages 2325–2328, 15-19 June 2008.